Journal of Power Sources 189 (2009) 149–154

Contents lists available at ScienceDirect

Journal of Power Sources

journal homepage: www.elsevier.com/locate/jpowsour

Flame co-synthesis of $LiMn_2O_4$ and carbon nanocomposites for high power batteries

T.J. Patey[a], R. Büchel[b], S.H. Ng[a], F. Krumeich[c], S.E. Pratsinis[b], P. Novák[a,*]

[a] Electrochemistry Laboratory, Paul Scherrer Institut, CH-5232 Villigen PSI, Switzerland
[b] Particle Technology Laboratory, Department of Mechanical and Process Engineering, ETH Zurich, Sonneggstrasse 3, ML F13, CH-8092 Zurich, Switzerland
[c] Laboratory of Inorganic Chemistry, ETH Zurich, Wolfgang-Pauli-Strasse 10, CH-8093 Zurich, Switzerland

ARTICLE INFO

Article history:
Received 28 July 2008
Received in revised form
24 September 2008
Accepted 1 October 2008
Available online 11 October 2008

Keywords:
$LiMn_2O_4$ nanoparticles
Carbon coating
Flame spray pyrolysis
High power lithium-ion battery

ABSTRACT

A novel method to produce $LiMn_2O_4$/carbon nanocomposites in a rapid, one-step and industrially scalable process is presented. A flame spray and a diffusion flame are combined to continuously produce $LiMn_2O_4$ nanoparticles and carbon black, respectively. Powder carbon content is varied by adjusting the diffusion flame conditions. The powders are characterized by X-ray diffraction (XRD), transmission electron microscopy, cyclic voltammetry and galvanostatic cycling for a range of current densities. These $LiMn_2O_4$/carbon nanocomposites retain over 80% of their initial galvanostatic discharge capacity for current densities ranging from 5 to 50C-rates, significantly better than pure $LiMn_2O_4$ nanoparticles mixed conventionally with commercial carbon blacks. The improved performance of the $LiMn_2O_4$/carbon nanocomposites is attributed to the carbon particle contact and/or film coating of the freshly-made $LiMn_2O_4$ nanoparticles. This additional well-distributed carbon provides an electrically conductive network that induces a more homogeneous charge transfer throughout the electrode. The suitability of these nanocomposites as a hybrid material is discussed by considering the layout of a thin-layer lithium-ion battery containing these flame-made nanocomposites as positive electrode and LiC_6 as negative electrode. The battery's specific energy is calculated to be 78 Wh kg^{-1} (50C-rate) based on the results of lithium-ion insertion capacity experiments and reasonable engineering assumptions on the lithium-ion battery design.

1. Introduction

One leading alternative cathode material to $LiCoO_2$ is $LiMn_2O_4$ for its lower cost, higher electrochemical potential vs. graphite, and its improved thermal stability [1–3]. High power applications such as electric vehicles require that lithium-ion batteries have a high specific power and energy [4,5]. One route to increase specific power is to significantly increase the interfacial area between electrochemically active material and electrolyte, thereby increasing the charge and discharge rates [6]. This opportunity has led many groups to develop nano-structured and/or nano-sized $LiMn_2O_4$ particles [7–10] and with promising results.

The full charge capacity of nano-sized cathode and anode materials cannot be realized if local electrical conductivity is insufficient for the given power demand. In other words, if an electrically conductive filler is not well dispersed throughout the active material, there will be parts of the active material which do not contribute to the capacity when a constant, high current is required. Therefore, sufficient dispersion of the electrically conductive additive amongst the active material is necessary for effective use. Carbon black (CB) is used commercially as an electrically conductive additive, either as a coating of the active material or as a powder dispersed throughout the active material. It is produced industrially by incomplete combustion of a gaseous or liquid hydrocarbon [11]. The lack of oxygen limits CO_2 formation and promotes CO, H_2 and carbon–carbon bond formation, contributing to the elemental carbon structure of CB.

Flame technology is used for CB production but is not a typical method for lithium-ion cathode material production. Our group has recently introduced flame spray pyrolysis (FSP) as a route to producing LiV_3O_8 [12] and $LiMn_2O_4$ nanoparticles [10] for use in lithium-ion batteries. Carbon-coated nanoparticles have been made by single flame combustion of $SiCl_4$ and acetylene [13] or hexamethyledisiloxane and H_2 [14] at production rates up to 700 g h^{-1}. Carbon-coated TiO_2 with or without soot (or CB) particles were made at high or low acetylene concentrations [15] in vapor-fed flames. Strobel et al. [16] made NO_x-storage reduction catalyst particles by two spray (liquid-fed) flame synthesis of separate Al_2O_3

* Corresponding author. Tel.: +41 56 310 2457; fax: +41 56 310 4415.
E-mail address: petr.novak@psi.ch (P. Novák).

0378-7753/$ – see front matter © 2008 Elsevier B.V. All rights reserved.
doi:10.1016/j.jpowsour.2008.10.002

and Pt/BaO or $Pt/BaCO_3$ nanoparticles. Ernst et al. have recently used flame technology for synthesis of platinum clusters embedded in CB by a one-step process [17]. They have also made Pt-clusters supported on CB by two separately staged spray flames: the first flame produced the CB particles while a second one downstream produced the Pt clusters that were scavenged onto the surface of the earlier formed co-flowing CB particles [17].

Vapor- and liquid-fed flame technology [15,17] is combined here to simultaneously make in one-step, for the first time to our knowledge, $LiMn_2O_4$/carbon nanocomposites for positive electrodes in lithium-ion batteries. Here, flame co-synthesis of $LiMn_2O_4$/carbon is presented and the electrochemical charge capacity of these materials at various specific currents (also known as C-rates) is shown. A description of the experimental method is given and an outlook of the benefits and challenges of this one-step synthesis of cathode material and its simultaneous carbon coating is presented.

2. Experimental

The precursor for synthesis of $LiMn_2O_4$ nanoparticles was prepared by mixing a 1:2 molar ratio of Li:Mn in an organic, combustible solution. More specifically, 4.5 g of Li–acetylacetonate (Aldrich) and 30.2 g of Mn(III)–acetylacetonate (Aldrich) were dissolved into 160 mL of 2-ethylhexanoic acid (Riedel-de Haën) and then 160 mL of Acetonitrile (Sigma–Aldrich, 99.5%) was added [10]. To ensure complete dissolution of the acetylacetonates, the solution was heated to 160 °C for 2 h while connected to a cooling reflux to ensure no mass loss.

The experimental set-up of FSP is described in detail elsewhere [18]. The liquid precursor was sprayed at a rate of 3 mL min^{-1} and dispersed by 5 L min^{-1} of oxygen. The spray was ignited by a support flame created by 1 L min^{-1} of methane and 3 L min^{-1} of oxygen. A pressure of 1.5 bar was maintained across the nozzle tip during synthesis. The spray flame (SF) nozzle was cooled by water to prevent overheating and precursor evaporation within the liquid feed lines. The carbon black was produced by supplying acetylene gas to the diffusion flame (DF) [13,17] using still air as oxidant prior to ignition of the flame spray. Hereafter, the diffusion flame-made carbon black produced in this work is referred to as DF–CB.

Four powders were produced: one with only $LiMn_2O_4$, two with varying $LiMn_2O_4$ and carbon content, and one with only DF–CB. The acetylene gas was supplied for production of these powders at 0, 0.5, 1.0, and 0.6 L min^{-1}, respectively. A schematic of the experimental set-up is shown in Fig. 1. Note that the distances and angle between the nozzles are provided.

Particles were collected on a glass-fiber filter (GF/D Whatman, 257 mm in diameter) placed 0.5 m directly over the flame or flames using a vacuum pump (Busch, Seco SV 1025). The Brunauer-Emmett-Teller (BET) specific surface area (SSA) of these powders was determined through a five-point nitrogen adsorption isotherm at 77 K (Tristar, Micrometrics Instruments Corp.) after degassing the samples with nitrogen at 150 °C for 90 minutes. The X-ray diffraction (XRD) measurements were performed using a Bruker AXS D8 Advance (40 kV, 40 mA) and analyzed with the Topas 2 software. The XRD measurement was performed at a continuous scan between 2θ angles of 10° and 70° at a scan rate of 0.03° min^{-1}. For the investigation by transmission electron microscopy (TEM), the material was deposited onto a holey carbon foil supported on a copper grid (Okenshoji Co., Ltd.). TEM investigations were performed using a CM30ST microscope (Philips; LaB_6 cathode, operated at 300 kV, point resolution ~2 Å).

The carbon content in the powders was measured thermogravimetrically in an oxidizing environment. Powder samples were heated up at a rate of 10 °C min^{-1} from room temperature up to 800 °C under 50 mL min^{-1} of air with the powder mass change

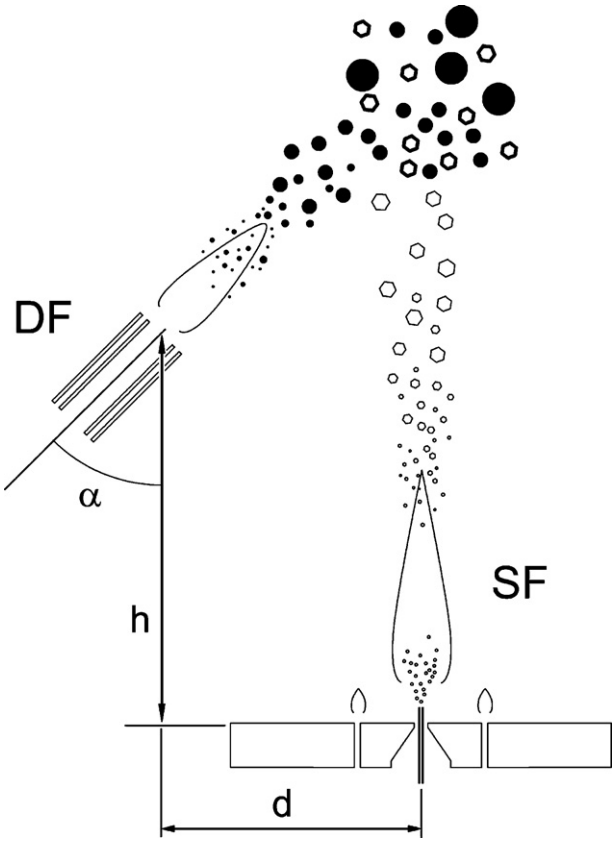

Fig. 1. Schematic of the co-synthesis of carbon black (DF–CB) and $LiMn_2O_4$ nanoparticles by a diffusion flame (DF) and a spray flame (SF), respectively. The distance between the nozzle tips are d = 5 cm and h = 9 cm. The angle between the nozzle axes is α = 45°.

measured via the Mettler Toledo TGA/SDTA851^e thermobalance. Electrodes made from the flame-produced powders, Super P (commercial CB, TIMCAL SA, BET SSA = 62 m^2 g^{-1}), and polyvinylidene fluoride (PVDF SOLEF 1015, Solvay) had a mass ratio of 7:2:1, respectively. They were prepared by first dispersing the flame-produced powder with the Super P in *N*-methylpyrrolidinone (NMP, Fluka) solvent. A solution of 10 wt.% PVDF dissolved in NMP was then mixed into the suspension to form a viscous slurry. The slurry is spread by doctor-blading at a thickness of 200 μm onto an aluminum foil and dried under vacuum at 110 °C overnight in order to remove the solvent and form a composite electrode.

Electrodes with a diameter of 13 mm were punched out and dried in a vacuum chamber at 120 °C overnight. They were then assembled in test cells similar to coin cells [19] where they function as working electrodes. Lithium metal (Aldrich, 99.9%) served as both counter and reference electrode. It was separated from the working electrode by a 1 mm thick fiberglass separator soaked in 500 μL of electrolyte [1 M $LiPF_6$ in ethylene carbonate (EC)/dimethyl carbonate (DMC) (1:1 by mass), Ferro GmbH]. Cells were assembled in an argon-filled glove box with less than 1 ppm of oxygen, water, and nitrogen contents.

Both cyclic voltammetry (CV) and galvanostatic measurements were performed by a computer-controlled cell capture (CCCC) system (Astrol Electronics AG, Oberrohrdorf, Switzerland) at 3.0–4.5 V vs. Li/Li^+ at a potential scan rate of 0.1 mV s^{-1}. For the rate capability experiments, the electrodes were cycled galvanostatically in the range of 3.5–4.3 V vs. Li/Li^+ for varying specific currents proportional to the mass of $LiMn_2O_4$. To quantify the contribution of the DF–CB's capacity, electrodes of DF–CB and PVDF were cycled and the capacity measured. The contribution

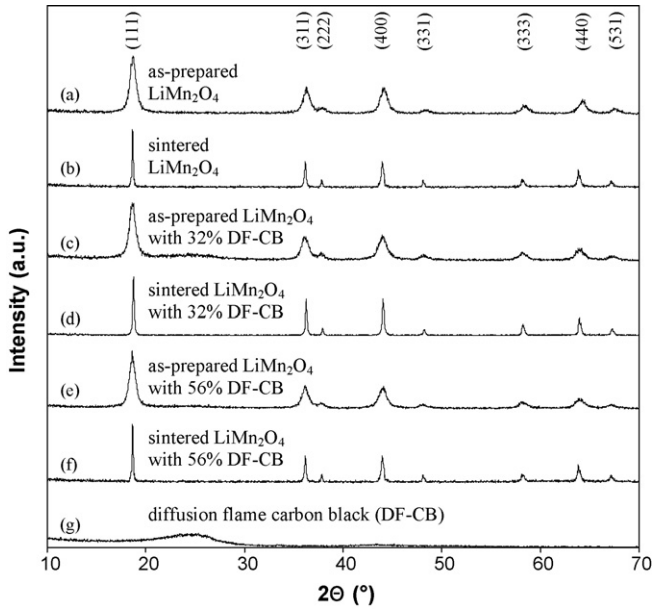

Fig. 2. XRD patterns of flame-produced powders before and after sintering up to 800 °C in air from room temperature. The *hkl* indices of $LiMn_2O_4$ planes are indicated. The powders are $LiMn_2O_4$ with wt.% DF–CB of (a) 0% as-prepared, (b) 0% after sintering, (c) 32% as-prepared, (d) 32% after sintering, (e) 56% as-prepared, and (f) 56% after sintering. The pattern of the powder with 100% DF–CB (g) is also presented.

of the CB's capacity is subtracted [20] from the capacity of the $LiMn_2O_4$/carbon nanocomposites. In order to promote complete discharge/charge at the respective potential limits, a potentiostatic step was included until the specific current dropped to 60 mA g^{-1}.

3. Results and discussion

Fig. 2 shows XRD patterns of the $LiMn_2O_4$ nanoparticles. The reflections are consistent with those of $LiMn_2O_4$ reported in literature [10,21]. No crystalline impurities are seen in these patterns. The diffuse scattering between roughly $2\Theta = 20$–30° that appears in the XRD patterns of powders produced with DF–CB (Fig. 2c,e) is attributed to the presence of amorphous carbon (Fig. 2g). Furthermore, no reflections of crystalline carbon (graphite) are seen, indicating that the carbon present is amorphous [13,15]. These amorphous patterns are no longer present after the powders were sintered at 800 °C in air following the thermogravimetric measurements and carbon oxidation.

The powders were thermogravimetrically measured to have a DF–CB mass composition of 0, 32, 56, and 100 wt.% and a SSA of 142, 117, 109, and 63 $m^2\,g^{-1}$, respectively. For the pure $LiMn_2O_4$ powder, this corresponds to an average particle diameter d_{BET} of about 10 nm, assuming a density of 4.3 g cm^{-3}. The crystal size is calculated to be 11 nm using the Scherrer equation indicating monocrystalline $LiMn_2O_4$. Fig. 3 shows images of these particles that are not always single as sintered necks between them are visible.

The decrease in SSA of the powders with carbon content might be due to an increase in mass of larger DF–CB particles. Although carbon is known to act as a particle growth inhibitor [22], there is no evidence that the presence of carbon has a significant effect on $LiMn_2O_4$ particle size as the XRD patterns a, c, and e in Fig. 2 indicate that the $LiMn_2O_4$ crystal size is nearly constant for all carbon contents. The reduction in SSA with carbon content most likely indicates coating of the high SSA FSP-made $LiMn_2O_4$ with carbon. Carbon-coated oxide nanoparticles have been observed in co-synthesis of SiO_2/carbon [13] and TiO_2/carbon [15] in vapor-fed flame reactors where the carbon first coats all existing surfaces and then starts to form separate soot particles. It is possible that a similar scenario is followed in this work, the co-synthesis of $LiMn_2O_4$/carbon (Fig. 1). The TEM images of Fig. 3b,c show an amorphous material, possibly DF–CB, particles or film attached to $LiMn_2O_4$ nanoparticles.

Fig. 4 shows cyclic voltammograms of the flame-made powders. The redox peaks for the electrode with pure $LiMn_2O_4$ (Fig. 4: thin line) is in close agreement with Ernst et al. [10]. The peaks for the $LiMn_2O_4$/carbon nanocomposites are narrower than pure $LiMn_2O_4$ due to the decreased overpotentials. Of course, the most important overpotential is the ohmic one. The additional carbon provides an electrically conductive network to induce a more homogeneous charge transfer throughout the electrode. In contrast, the broader peaks of the electrode without DF–CB (although Super P is present in the electrode) indicate that the overall charge transfer is slower than in the other two electrodes. The overpotential for both the redox pairs in the $LiMn_2O_4$/carbon electrodes is then lower when compared to the pure $LiMn_2O_4$ electrode. The overpotentials only slightly decrease when the DF–CB content was increased from 32 (Fig. 4: thick line) to 56 wt.% (Fig. 4: dashed line). This indicates that for the low scan rate of 0.1 mV s^{-1} nearly equilibrium behavior has been achieved in both electrodes. This could be attributed to the beneficial effect of carbon coating of the $LiMn_2O_4$ nanoparticles (Fig. 3b,c). As the additional DF–CB had only a slight influence on the overall charge transfer rate, additional DF–CB made little or no influence at that scan rate. This could be because the increase in C_2H_2 gas concentration and carbon content did not increase the carbon layer thickness. Indeed, separate carbon particles were formed, cf. Fig. 3a. Vapor-fed carbon layers 2–3 nm thick on TiO_2 did not become thicker with increasing C_2H_2 concentration and carbon content, only additional soot particles were formed [15].

The cycle life behavior of the flame-made powders for various C-rates illustrates the importance of an electrically conductive network for nanoparticles. These results are displayed in Fig. 5. Here 1C-rate is equivalent to 148 A kg^{-1}. To accurately compare the electrodes, the contribution of the charge capacity of the DF–CB has been accounted for. Cycling of electrodes composed of DF–CB and PVDF indicates that the contribution of the DF–CB is roughly 2 Ah kg^{-1} (per unit mass flame-made CB). Despite this relatively low value, the DF–CB present reacts with the electrolyte in an irreversible oxidative reaction due to the high voltage (>4 V) [20]. This possibly contributes to capacity fading due to decomposition of the electrolyte.

As the C-rate increases, there is a sharp decrease in the electrochemical performance of the powder produced without any DF–CB present, even though there is 20 wt.% of Super P present in the electrode. This is especially apparent when C-rates are greater than or equal to 5C-rate, where the sharp decline in discharge capacity (or lithium-ion insertion) is attributed to insufficient local electrical contact between the $LiMn_2O_4$ nanoparticles and the Super P. In addition, it is seen in the inset of the Fig. 5 that both the electrodes with DF–CB retained more than 80% of their nominal discharge capacities, even when cycled up to a 50C-rate (~70 s in discharge time). This result is partly attributed to the carbon coating seen on some of the $LiMn_2O_4$ nanoparticles (Fig. 3b,c). In contrast, the pure $LiMn_2O_4$ electrode could only retain above 80% of its nominal discharge capacity when cycled up to a 2C-rate (~30 min in discharge time). This improvement in rate capability of more than 20 times shows that improved electrical contact in the electrode is necessary for high power lithium-ion battery application.

While the results of the lithium-ion insertion capacity experiments show a reasonable capacity per unit mass $LiMn_2O_4$, the large amount of carbon present (>30%) makes these nanocomposites

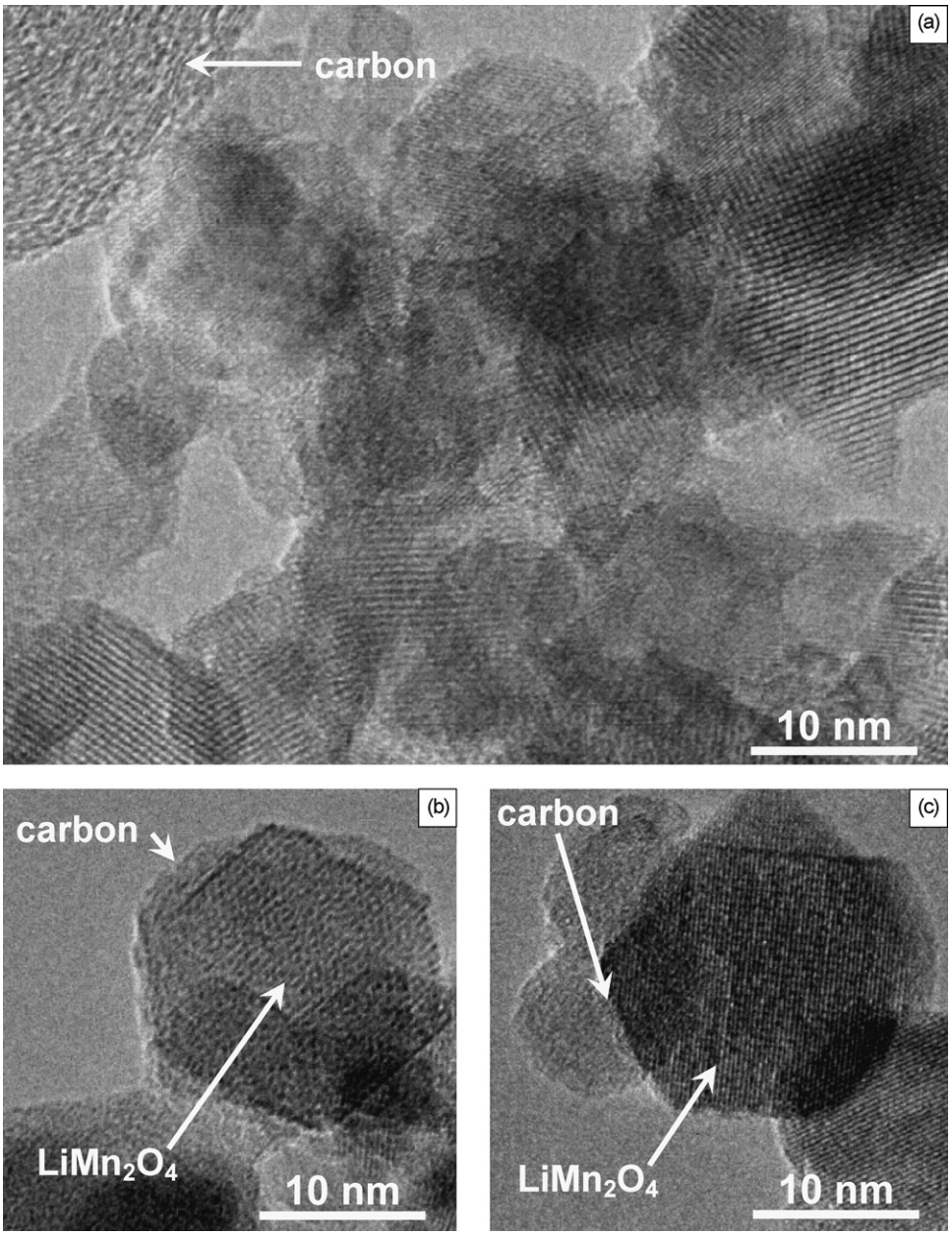

Fig. 3. TEM images of (a) $LiMn_2O_4$/carbon nanocomposites (32 wt.% DF–CB) depicting (b) amorphous carbon films and (c) particles attached to $LiMn_2O_4$ crystalline particles.

unsuitable for high energy applications. The carbon content, however, can be easily reduced during synthesis of such nanocomposites [15]. Even so, the relatively high lithium-ion insertion capacity at 50C-rate (>80 Ah kg^{-1}) of the nanocomposites would make the hybrid material suitable for high power applications and competitive to electrochemical supercapacitors. This highlights the necessity of optimizing an electrode's carbon content for the power density required of the application.

To support the argument that these nanocomposites used in lithium-ion batteries would be competitive to electrochemical supercapacitors, a layout of a battery containing the nanocomposites is investigated. The specific energy of a spirally-wound, cylindrical thin-layer lithium-ion cell is calculated based on typical battery material data and reasonable engineering assumptions [23,24]. As a counter electrode a standard graphite electrode is assumed here [24]. Of course, in a practical device it will have to be replaced with a high rate one but such a replacement will certainly not decrease the energy density of the battery by an order of magnitude.

A typical internal configuration of such a cell is shown in Fig. 6. The thickness of this stack is about 0.3 mm, assuming the aluminum foil, copper foil, and each polymer separator foil have a thickness of 10 μm each. The positive electrode is a composite of the flame-made powder ($LiMn_2O_4$ with 32 wt.% DF–CB), Super P, and PVDF, as used in the lithium-ion insertion capacity experiment shown in Fig. 5. Because the electrode is designed for high power, it is assumed to have a porosity of 50% filled with the electrolyte [24]. Based on the results of the lithium-ion insertion capacity experiment (Fig. 5) at 50C-rate, a lithium-ion insertion capacity of 41 Ah kg^{-1} (per unit mass electrode material with electrolyte-filled pores) is used for the calculations. The negative electrode is assumed to have a lithium-ion insertion capacity of 220 Ah kg^{-1} based on reasonable engineering assumptions [24]. The average cell voltage of a $LiMn_2O_4/LiC_6$ couple is about 3.6 V on

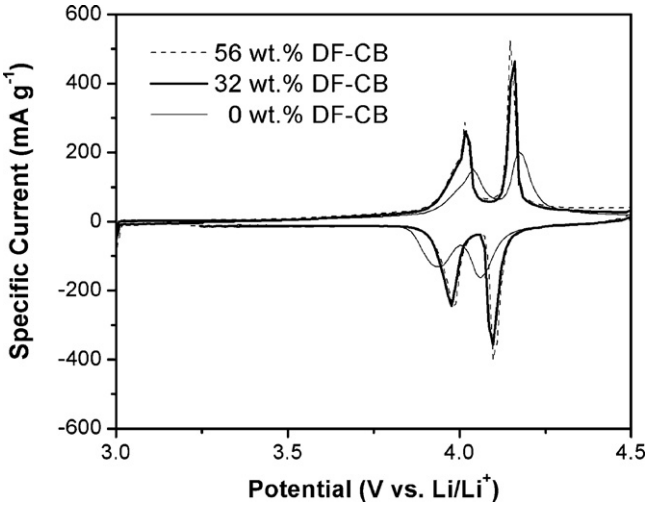

Fig. 4. Cyclic voltammograms of $LiMn_2O_4$ powders containing various contents of co-produced carbon black in the 1st cycle at 0.1 mV s^{-1}.

discharge [23]. The product of this voltage and the calculated specific charge of 27 Ah kg^{-1} is 97 Wh kg^{-1} and is the specific energy of the hypothetical cell without any containment. Assuming the cell's housing would be 20% of the total battery's mass [24], the specific energy of the battery would be 78 Wh kg^{-1}. The specific energy of today's practical supercapacitors is less than 10 Wh kg^{-1} [25,26]. The specific energy of the battery with the nanocomposite is thus almost one order of magnitude higher than that of a supercapacitor.

The energy is deliverable at a C-rate of 50. The high current density is possible due to the small Li-diffusion pathways to the active sites of the $LiMn_2O_4$ nanoparticles and due to the high and uniform local electrical conductivity of the carbon present. The nanocomposites balance power with energy density, are a possible replacement of supercapacitors, and could also fill a niche between the high energy density of lithium-ion batteries and the high power density of supercapacitors.

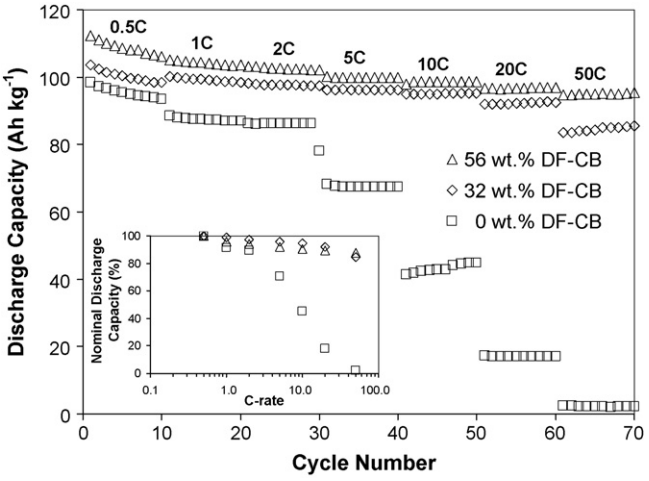

Fig. 5. Lithium-ion insertion (discharge) capacities for electrodes with the FSP-produced $LiMn_2O_4$ nanoparticles and various co-produced carbon black contents at various C-rates with cut-off potentials of 3.5 and 4.3 V vs. Li/Li^+. A 1C-rate is assumed to be 148 A kg^{-1} and both the C-rates and the discharge capacity are based on the mass of $LiMn_2O_4$ in the electrode. Only the galvanostatic part of the respective cycle is considered here. Inset shows the nominal discharge capacities of the above materials, based on the average of 10 cycles at the given C-rate.

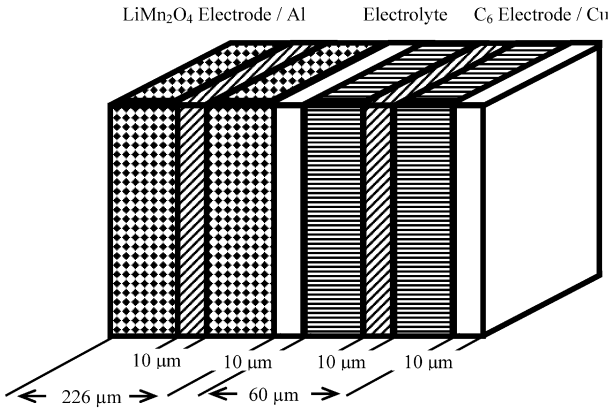

	µm	mg cm^{-2}	mAh cm^{-2}
LiC_6 (composite 220 Ah kg^{-1})	50	8.4	1.8
$LiMn_2O_4$ (composite 41 Ah kg^{-1})	216	45.5	1.8
Separators	20	2.0	
Al - Sheet	10	2.7	
Cu - Sheet	10	8.9	
Total	306	67.5	1.8

Average density	2.2 g cm^{-3}
Average charge capacity	60 mAh cm^{-3}
Specific charge	27 Ah kg^{-3}
Average voltage	3.6 V
Specific energy (without containment)	97 Wh kg^{-1} (50C-rate)
Specific energy	**78 Wh kg^{-1} (50C-rate)**

Fig. 6. Layout of a lithium-ion cell and typical data combined with discharge capacity data of the $LiMn_2O_4$/carbon nanocomposite (32 wt.% DF–CB).

4. Conclusions

A novel method for synthesis of $LiMn_2O_4$/carbon electroactive nanocomposites is presented. The core structure of this nanocomposite material is $LiMn_2O_4$ nanoparticles coated with carbon particles or films that have been formed by surface growth. This one-step, co-synthesis process is important towards carbon coating of nanoparticles for powders with less than 5 wt.% carbon which would be suitable for high energy lithium-ion batteries. For nanoparticles to be used effectively in high power lithium-ion batteries, a sufficient electrically conductive network should be present to deliver the energy needed at the current density required. Such a network is present in the $LiMn_2O_4$/carbon nanocomposites. These composites had a considerably higher specific galvanostatic discharge capacity at a 5C-rate or greater than the electrode with powder of pure $LiMn_2O_4$. The significance of these results is illustrated by calculation of the specific energy of a thin-layer lithium-ion battery containing the flame-made $LiMn_2O_4$/carbon nanocomposite as positive electrode and LiC_6 as negative electrode (78 Wh kg^{-1} at 50C-rate). If the nanocomposites were used in a lithium-ion battery, such a device could replace supercapacitors in high power applications for durations longer than supercapacitors could sustain.

Acknowledgements

Continuous support from and scientific discussions with Prof. A. Wokaun (PSI and ETH Zurich) are greatly appreciated. Technical assistance of Mr. W. Scheifele (PSI) and Mr. H. Kaiser (PSI) is highly appreciated. TEM images were acquired at the Electron Microscopy ETH Zurich (EMEZ). This research was partially funded by the ETH Research Grant TH-29/05-2 and TH-09/06-2 (R. Büchel).

References

[1] M.M. Thackeray, W.I.F. David, P.G. Bruce, J.B. Goodenough, Mater. Res. Bull. 18 (1983) 461–472.
[2] R.J. Gummow, A. Dekock, M.M. Thackeray, Solid State Ionics 69 (1994) 59–67.
[3] M. Lanz, C. Kormann, H. Steininger, G. Heil, O. Haas, P. Novák, J. Electrochem. Soc. 147 (2000) 3997–4000.
[4] M. Saft, G. Chagnon, T. Faugeras, G. Sarre, P. Morhet, J. Power Sources 80 (1999) 180–189.
[5] Y. Tanjo, T. Abe, H. Horie, T. Nakagawa, T. Miyamoto, K. Katayama, Soc. Automot. Eng. (Spec. Publ.) SP-1417 (1999) 51–55.
[6] A.S. Arico, P. Bruce, B. Scrosati, J.M. Tarascon, W. van Schalkwijk, Nat. Mater. 4 (2005) 366–377.
[7] S.H. Park, S.T. Myung, S.W. Oh, C.S. Yoon, Y.K. Sun, Electrochim. Acta 51 (2006) 4089–4095.
[8] J.Y. Luo, L. Cheng, Y.Y. Xia, Electrochem. Comm. 9 (2007) 1404–1409.
[9] Z. Bakenov, M. Wakihara, I. Taniguchi, J. Solid State Electrochem. 12 (2008) 57–62.
[10] F.O. Ernst, H.K. Kammler, A. Roessler, S.E. Pratsinis, W.J. Stark, J. Ufheil, P. Novák, Mater. Chem. Phys. 101 (2007) 372–378.
[11] M. Kühner, G. Voll, in: J.-B. Donnet, R.C. Bansal, M.-J. Wang (Eds.), Carbon Black Science and Technology, 2nd ed., Marcel Dekker, New York, 1993, pp. 1–65.
[12] T.J. Patey, S.H. Ng, R. Buechel, N. Tran, F. Krumeich, J. Wang, H.K. Liu, P. Novák, Electrochem. Solid-State Lett. 11 (2008) A47–A50.
[13] P.T. Spicer, C. Artelt, S. Sanders, S.E. Pratsinis, J. Aerosol Sci. 29 (1998) 647–659.
[14] H.K. Kammler, R. Mueller, O. Senn, S.E. Pratsinis, AIChE J. 47 (2001) 1533–1543.
[15] H.K. Kammler, S.E. Pratsinis, J. Mater. Res. 18 (2003) 2670–2676.
[16] R. Strobel, L. Mädler, M. Piacentini, M. Maciejewski, A. Baiker, S.E. Pratsinis, Chem. Mater. 18 (2006) 2532–2537.
[17] F.O. Ernst, R. Buechel, R. Strobel, S.E. Pratsinis, Chem. Mater. 20 (2008) 2117–2123.
[18] L. Mädler, H.K. Kammler, R. Mueller, S.E. Pratsinis, J. Aerosol Sci. 33 (2002) 369–389.
[19] P. Novák, W. Scheifele, F. Joho, O. Haas, J. Electrochem. Soc. 142 (1995) 2544–2550.
[20] L. Fransson, T. Eriksson, K. Edstrom, T. Gustafsson, J.O. Thomas, J. Power Sources 101 (2001) 1–9.
[21] M.M. Thackeray, P.J. Johnson, L.A. de Picciotto, P.G. Bruce, J.B. Goodenough, Mater. Res. Bull. 19 (1984) 179–187.
[22] S.H. Ng, J. Wang, D. Wexler, S.Y. Chew, H.K. Liu, J. Phys. Chem. C 111 (2007) 11131–11138.
[23] O. Haas, E. Deiss, P. Novák, W. Scheifele, A. Tsukada, in: C.F. Holmes, A.R. Landgrebe (Eds.), Proceedings of the Symposium on Batteries for Portable Applications and Electric Vehicles, The Electrochemical Society Proceedings Series, Pennington, NJ, 1997, pp. 451–462.
[24] D. Haringer, P. Novák, O. Haas, B. Piro, M.C. Pham, J. Electrochem. Soc. 146 (1999) 2393–2396.
[25] R. Kotz, M. Carlen, Electrochim. Acta 45 (2000) 2483–2498.
[26] P. Simon, A. Burke, ECS Interface, Spring (2008) 38–43.